Journal of Chromatography A, 1216 (2009) 7375–7383

Contents lists available at ScienceDirect

Journal of Chromatography A

journal homepage: www.elsevier.com/locate/chroma

Sol–gel synthesis of macro–mesoporous titania monoliths and their applications to chromatographic separation media for organophosphate compounds

Junko Konishi[a], Koji Fujita[a,b,*], Kazuki Nakanishi[c], Kazuyuki Hirao[a], Kei Morisato[d], Shota Miyazaki[d], Masayoshi Ohira[d]

[a] Department of Material Chemistry, Graduate School of Engineering, Kyoto University, Nishikyo-ku, Kyoto 615-8510, Japan
[b] PRESTO, Japan Science and Technology Agency (JST), 4-1-8, Honcho Kawaguchi, Saitama, Japan
[c] Department of Chemistry, Graduate School of Science, Kyoto University, Oiwake-cho, Kitashirakawa, Sakyo-ku, Kyoto 606-8502, Japan
[d] GL Sciences Inc., 237-2 Sayamagahara, Iruma, Saitama 358-0032, Japan

ARTICLE INFO

Article history:
Available online 10 June 2009

Keywords:
Titania monoliths
HPLC separation media
Hierarchically porous structure
Organophosphate compounds
Sol–gel method
Phase separation

ABSTRACT

We have developed a method of independently tailoring the macro- and mesoporous structures in titania (TiO_2) monoliths in order to achieve liquid chromatographic separations of phosphorous-containing compounds. Anatase TiO_2 monolithic gels with well-defined bicontinuous macropores and microstructured skeletons are obtained via the sol–gel process in strongly acidic conditions using poly(ethylene oxide) as a phase separator and *N*-methylformamide as a proton scavenger. Aging treatment of the wet gels in the mother liquor at temperatures of 100–200 °C and subsequent heat treatment at 400 °C allow the formation and control of mesoporous structures with uniform pore size distributions in the gel skeletons, without disturbing the preformed macroporous morphology. The monolithic TiO_2 rod columns with bimodal macro–mesoporous structures possess the phospho-sensitivity and exhibit excellent chromatographic separations of phosphorus-containing compounds.

1. Introduction

In the last decade, monolithic columns consisting of single piece of an organic polymer or silica (SiO_2) with flow-through pores are increasingly recognized as a viable alternative to microparticulate packed columns in high-performance liquid chromatography (HPLC) and capillary electrochromatography (CEC) [1,2]. Because of the high permeability of monolithic columns, long columns can be utilized to enhance the separation efficiency (plate numbers). In addition, high-speed separation is feasible due to the compatibility of monoliths with high flow rates. Utilizing these two features, monolithic separation media have found applications in the areas such as high-throughput screening and the separation of complex mixtures. In particular, SiO_2-based monolithic columns developed by Nakanishi [3] represent an outstanding achievement in this field. The synthesis process is based upon alkoxy-derived sol–gel reactions in the presence of water-soluble organic polymers, such as poly(ethylene oxide). During the polymerization reaction of silicon alkoxides in an acidic condition, spinodal decomposition-type phase separation occurs concurrently with gelation, resulting in the formation of bicontinuous SiO_2-rich and solvent-rich phases on the length scale of micrometers. Subsequent solvent exchange with a basic aqueous solution and thermal treatment, i.e., aging treatment in hydrothermal conditions, generates the mesopores in the SiO_2-rich phase via a process of dissolution/reprecipitation (Ostwald ripening). Upon evaporation drying, the SiO_2-rich phase becomes mesoporous SiO_2 skeletons, and the solvent-rich phase turns into macropores that serve as flow-through pores. The macropores allows facile transport of fluid, while the mesopores enlarge the surface area that assists the contacts the fluid and the solid surface. Consequently, the monolithic SiO_2 columns with a bimodal porous structure have been shown to provide high efficiencies at high flow rates, unlike conventional packed columns [4,5].

Another current trend in the development of new stationary phases is the use of microparticulate packed columns based on metal oxides other than SiO_2. Titania (TiO_2) and zirconia (ZrO_2) have been extensively studied as chromatographic support materials because of their excellent pH and thermal stability and great mechanical strength compared to SiO_2 [6,7]. TiO_2 and ZrO_2 also have amphoteric hydroxide groups on their surfaces so that they can be either cation- or anion-exchangers depending on pH, while SiO_2 behaves only as a cation exchange [8]. Thus, enhanced chromatographic performances are expected to arise from TiO_2- and ZrO_2-based supporting materials. Another unique advantage of using TiO_2 or ZrO_2 as the support material is their ability to selectively adsorb organophosphate compounds [9–12], which can be

* Corresponding author. Tel.: +81 75 383 2432; fax: +81 75 383 2420.
E-mail address: fujita@dipole7.kuic.kyoto-u.ac.jp (K. Fujita).

0021-9673/$ – see front matter © 2009 Elsevier B.V. All rights reserved.
doi:10.1016/j.chroma.2009.06.016

used to selectively enrich or isolate phosphate compounds and phosphorylated proteins and peptides [13–23].

Although the benefits of non-SiO_2 metal oxides as a support material, as well as the fortes of the monolithic format as a chromatographic column, have been established, only very few attempts have been made to develop monolithic TiO_2 and ZrO_2 columns, due primary to the absence of versatile synthesis strategies as demonstrated for SiO_2 systems. An initial approach toward the development of monolithic non-SiO_2 columns was to modify the skeleton surfaces of SiO_2 monoliths. For example, Shi et al. [24] prepared ZrO_2-coated SiO_2 monoliths in fused SiO_2 capillaries and applied them to CEC. Miyazaki et al. [25] reported the similar method to obtain monolithic SiO_2 columns coated with TiO_2, and showed the possibility of HPLC separations for phosphorylated compounds. Recent progresses have been made in the synthesis of pure TiO_2 and ZrO_2 monoliths [26–31]. Konishi et al. [29,30] developed reliable and reproducible synthesis pathways to fabricate TiO_2 and ZrO_2 monoliths with bimodal macro–mesoporous structures utilizing the alkoxy-derived sol–gel process accompanied by phase separation. Using the phase separation route, monolithic TiO_2 and ZrO_2 columns were also produced in fused SiO_2 capillaries so that the chromatographic separations could be demonstrated [32,33].

These attempts toward chromatographic applications of pure TiO_2 and ZrO_2 monoliths, however, need more investigations. An important factor in the development of monolithic columns is feasibility of controlling macro- and mesoporous structures independently, which may be useful in improving the chromatographic performance as evidenced for monolithic SiO_2 columns [2,3]. Although the phase separation route in sol–gel synthesis assures the formation and control of macropores, the methods of tailoring mesopores have not yet been fully explored, especially for TiO_2 systems. Thus, challenge arises as to how to control the mesoporous structures in TiO_2 monoliths. Shrinkage of gels during the synthesis is another critical issue in the achievement of chromatographic separation using monolithic columns, because it is often accompanied by deformation of monolithic shape and/or crack formation in the skeletons, which would result in the deterioration of column efficiency or in extremely cases, the failure of separation, due to the inhomogeneous fluid flow. Since the shrinkage is an inevitable phenomenon encountered in the sol–gel synthesis, the size reduction of the whole structure must be managed so that the macroscopic shape can be retained.

In this paper, we describe a synthesis pathway to form TiO_2 monoliths suitable for the chromatographic use. By modifying the starting compositions in the alkoxy-derived sol–gel reactions as described previously [28] and applying the thermal treatment in the aging stage of wet gels, one can obtain the uniform and crack-free TiO_2 monoliths that possess bimodal pore size distributions with adjustable sizes in the macro- and mesopore regimes. We also demonstrate HPLC separation properties of phosphorus-containing compounds using the monolithic TiO_2 columns encased in an FEP poly(tetrafluoroethylene) tubing.

2. Experimental

2.1. Chemicals

Titanium propoxide ($Ti(O^nPr)_4$) and poly(ethylene oxide) (PEO) with a number-average molecular weight (M_n) of 10,000 were purchased from Aldrich (St. Louis, MO, USA). 35 wt% aqueous solution of hydrochloric acid (HCl) and *N*-methyl formamide (NFA) were obtained from Hayashi Pure Chemical Ind., Ltd. (Japan) and Wako Pure Chemical Ltd. (Japan), respectively. Adenosine, adenosine 5′-monophosphase (AMP), adenosine 5′-diphosphate (ADP), and adenosine 5′-triphosphate (ATP) were obtained from Sigma (St. Louis, MO, USA). Water (H_2O) was distilled and deionized using a Millipore Milli-Q system (Bedfold, MA, USA). All other reagents were of analytical grade and purchased from Kishida Chemical Co., Ltd. (Japan).

2.2. Instrumentation

The micrometer-range morphology of TiO_2 monoliths was observed by scanning electron microscope (SEM; S-2600N, Hitachi Ltd., Japan). The pore size distribution of gel samples was determined by mercury porosimetry (PORESIZER-9320, Micromeritics, USA) and nitrogen adsorption–desorption (TriStar 3000, Micromeritics, USA) methods. For nitrogen sorption, the pore size distribution in the micro- and mesoporous regimes was calculated by the Barrett–Joyner–Halenda (BJH) method using the adsorption branch of the isotherm. The specific surface area was obtained according to the Brunauer–Emmet–Teller (BET) method. X-ray diffraction (XRD) analysis with Cu K_α radiation (Rint2500, Rigaku Co., Japan) was performed to identify the crystalline phase precipitated. The measurements were made on the powder specimens prepared by grinding the monolithic gels. The crystallite size was calculated by the Scherrer's equation using the full width at half maximum of diffraction peaks of crystalline phase.

2.3. Chromatographic condition

HPLC experiments were performed with a GL-7410 pump (GL Sciences, Tokyo, Japan), a GL-7450 UV/VIS detector, a model 7725i sample injector (Rheodyne, USA), and a GL-7430 column oven. Data acquisition and processing were performed by an EZchrom Elite Chromatography Data System ver. 3.1.7J (Agilent Technologies, CA, USA). A mixture of 100 mM phosphate buffer (pH 6.5) and acetonitrile (40:60) was employed as eluent, where the phosphate buffer was prepared from sodium dihydrogenphosphate dihydrate and disodium hydrogenphosphate heptahydrate. As a standard sample, 1 mg each of adenosine, AMP, ADP, and ATP was dissolved in eluent, and then each sample concentration was mixed at 0.25 mg/ml.

2.4. Materials synthesis

All the starting compositions used in this study are listed in Table 1. The molar ratio was $Ti(O^nPr)_4$:H_2O:HCl:NFA = 1:4:0.55:*f*, where *f* = 0.725, 0.750, and 0.775. In the present experiment, only the amount of NFA was varied in order to control the micrometer-range morphology of gels. Hereafter, the NFA/$Ti(O^nPr)_4$ molar ratio, *f*, will be often utilized to distinguish the gel samples prepared with different NFA contents. The detail of gel preparation is as follows. First, the aqueous solution containing HCl, PEO, and NFA was added to $Ti(O^nPr)_4$, stirring under an ice-cooled condition. After stirring for 4 min, the transparent solution was poured into a polypropylene tube. Then, the tube was sealed and kept at 60 °C for gelation and phase separation. The resultant gel was aged at the same temperature for 24 h. In some cases, the gel, together with the mother liquor, was transferred to a stainless-steel autoclave with a Teflon inner liner and additionally aged at different temperature of 100–200 °C for 24 h under an autogeneous pressure in order to tailor the micro- and mesoporous structures. The wet gel thus obtained was solvent-exchanged with 1-propanol and evaporation-dried at 40 °C for 1 week. The solvent exchange prior to the drying process was per-

Table 1
Typical starting compositions to produce monolithic TiO_2 gels.

$Ti(O^nPr)_4$ (g)	35 wt% HCl aq. (ml)	H_2O (g)	NFA (ml)	PEO (M_n = 10,000) (g)
34.807	5.827	4.181	5.178	1.05
34.807	5.827	4.181	5.356	1.05
34.807	5.827	4.181	5.535	1.05

formed to reduce the capillary force developed during the drying step. Some of the dried gels were heat-treated at 400 °C for 5 h in air to enhance the crystallinity; heat treatment to this temperature was also necessary to remove the organic compounds almost completely, according to the results of thermogravimetry and differential thermal analysis.

In order to characterize the monolithic TiO_2 gels as a separation medium, we also performed the gel synthesis in a polypropylene tube of 4 mm inner diameter (ID) and 200 mm length. The TiO_2 rod cut to 50 mm in length was covered with a heat-shrinking FEP poly(tetrafluoroethylene) tube and set to a stainless-steel empty column (4.6 mm ID × 50 mm length, GL Sciences) through epoxy resin EPICLON (DIC Corporation, Tokyo, Japan).

3. Results and discussion

3.1. Formation and control of macroporous structure

In our previous work [29], monolithic TiO_2 gels were prepared via the hydrolysis and polycondensation reaction of $Ti(O^nPr)_4$ in the presence of formamide (FA) under a strongly acidic condition. In the $Ti(O^nPr)_4$–FA system, the gelation was controlled by a stepwise increase in the solution pH due to the hydrolysis of FA in the strong acid, while the phase separation was driven by the reduction in compatibility between the polymerizing TiO_2 oligomers and the polar solvent containing FA. In the present study, we modify the composition of the starting solution for the purpose of improving the mechanical strength of the gel skeletons. A large difference in the starting composition between the present and previous works is the concentration of $Ti(O^nPr)_4$; the concentration of $Ti(O^nPr)_4$ used in this study is about 67 wt%, which is larger than that used in the previous study (~47 wt%). The higher concentration of $Ti(O^nPr)_4$ is expected to strengthen the gel skeletons through the increased stiffness, thereby making them better able to resist capillary stresses developed during evaporation drying and heat treatment. In the more concentrated system, however, the reactivity of precursor solution becomes too high to control the gelation. Here, we employ NFA as the acid scavenger to control the gelation, instead of using FA; in the presence of strong acid, NFA is more slowly hydrolyzed than FA due to the N substitution, and hence, the solution pH raises more gently, which enables to control the gelation even in the concentrated systems. On the other hand, a larger amount of propanol generated in the hydrolysis of the more concentrated sol–gel systems reduces the phase-separation tendency because amphiphilic and low-molecular propanol works as a good solvent for TiO_2 oligomers. Indeed, the gels prepared from the PEO-free system were colorless and transparent, meaning rather weak phase-separation tendency. Therefore, a water-soluble polymer, i.e., PEO, is newly added to the starting solution as the phase separator. Since PEO adsorbs preferentially to TiO_2 oligomers via hydrogen bonding [34], the hydrophobic–hydrophilic repulsive interaction that drives the phase separation is expected to work between solvent mixtures and PEO adsorbed on TiO_2 oligomers, as reported for PEO-incorporated alkoxy-derived SiO_2 [3] and ZrO_2 [30] sol–gel systems. Careful design of the starting composition in $Ti(O^nPr)_4$–NFA–PEO system makes it possible to produce TiO_2 monoliths with bicontinuous morphology on the length scale of micrometers as a consequence of the polymerization-induced phase separation and nearly concurrent gelation. Fig. 1 displays the micrometer-range morphology of the dried gels prepared with $f = 0.725$, 0.750, and 0.775. The aging treatment was performed only at 60 °C. A bicontinuous configuration is observed with the TiO_2-derived skeletons and macropores interconnected to form a three-dimensional network. This kind of morphology, including the smooth skeleton surface, is typical of structures developed by spinodal decomposition [3]. We also confirmed that the heat treatment at 400 °C to remove residual organic compounds has only little influence on the macroporous morphology.

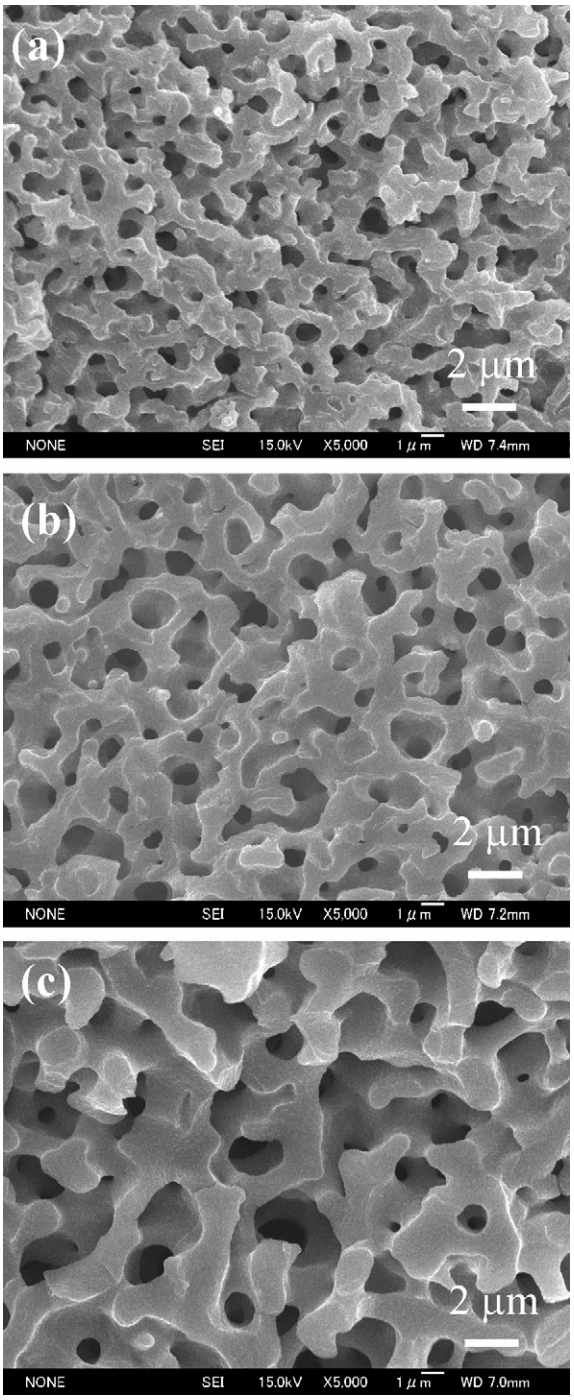

Fig. 1. SEM images of the dried gels prepared with $f = 0.725$ (a), 0.750 (b), and 0.775 (c). These dried gels were derived via the aging treatment at 60 °C. The scale bars correspond to 2 μm.

It is also seen from Fig. 1 that the sizes of gel skeletons and macropores increase with increasing the amount of NFA in the starting composition. The macroporous morphology is determined by the timing of the onset of phase separation relative to gelation, since the spinodal decomposition involves a coarsening process of phase-separated structures. In the present system, the gelation time remains almost unchanged with increasing NFA content, presumably because the accelerated effect of gelation caused by more rapid pH rise competes with the retardation effect of gela-

tion originated from the dilution of $Ti(O^nPr)_4$. On the other hand, it is anticipated that an increase in the fraction of polar solvent, i.e., NFA, in the starting composition enhances the repulsive interaction between gel phase and solvent phase during the polymerization reaction, thereby accelerating the onset of phase separation. The increase in pore size with the increase in the amount of NFA, as shown in Fig. 1, can be thus explained in terms of the enhanced phase separation. Here, it should be noted that varying the amount of phase separator, i.e., PEO, in the starting composition also has great impact on the macroporous morphology, because it essentially controls the phase-separation tendency. As the amount of PEO was increased in the starting composition, more coarsened bicontinuous macroporous morphologies were obtained, due to the enhanced phase-separation tendency. The detailed results will be reported elsewhere.

3.2. Control of mesoporous structure

As we reported previously for the $Ti(O^nPr)_4$–FA system [29], the addition of strong acid such as HCl to the starting composition promotes the hydrolysis of $Ti(O^nPr)_4$ but retards the polycondensation reaction. In the polycondensation stage, the slow and homogeneous increase in solution pH caused by the hydrolysis of FA allows the uniform formation of alkoxy-derived oligomers, which link together to produce a sol of primary particles that subsequently cross-link through the condensation among the surface hydroxyl groups to give a monolithic gel. In addition, the delayed condensation reaction tends to favor the structural arrangement into anatase-type crystalline TiO_2, although the crystallinity is rather poor. As a result, the dried gels derived from the $Ti(O^nPr)_4$–FA system were observed to possess the skeletons composed of agglomerated anatase nanoparticles with inter-particle voids (typically 1–2 nm) [35]. The dried gels synthesized from the present $Ti(O^nPr)_4$–NFA–PEO system in the presence of HCl are also expected to have similar microstructure and crystallinity unless the original wet gels are subjected to any special post-gelation treatments. Here, we have investigated the effects of the post-gelation processes, such as aging treatment and heat treatment, on the crystallinity and textural properties of gel skeletons. For this investigation, after the gelation at 60 °C, the wet gel was subjected to one of following procedures: (i) aged in the mother liquor at the same temperature as that for gelation (i.e., 60 °C) for 24 h or (ii) aged in the mother liquor at 60 °C for 24 h and then additionally aged at selected temperatures ranging from 100 to 200 °C for 24 h. After either treatment of (i) or (ii), the resultant wet gels were solvent-exchanged with 1-propanol and evaporation-dried at 40 °C. Some of the dried gels were further heat-treated at 400 °C in air in order to achieve the high crystallinity and also to eliminate the organic residuals.

XRD measurements were performed for the dried and heat-treated gels prepared with $f = 0.750$ and aged at different temperatures in order to evaluate the evolution of the crystallinity of gel skeletons during the aging treatment and/or heat treatment. Typical XRD patterns are shown in Fig. 2a and b for the dried and heat-treated gels derived via aging at 60 °C and those via aging at 200 °C, respectively. Anatase-type TiO_2 is found to be the main crystalline phase present in all the samples, although the anatase peaks for the dried gel derived via aging at 60 °C are rather broad. A minor brookite peak is also detected for the dried and heat-treated gels obtained after the aging treatment at 200 °C. In Fig. 2c, the crystallite size estimated from the anatase 1 0 1 diffraction peak according to Scherrer's equation is plotted as a function of aging temperature.[1] For the dried gels, the crystallite size depends on the

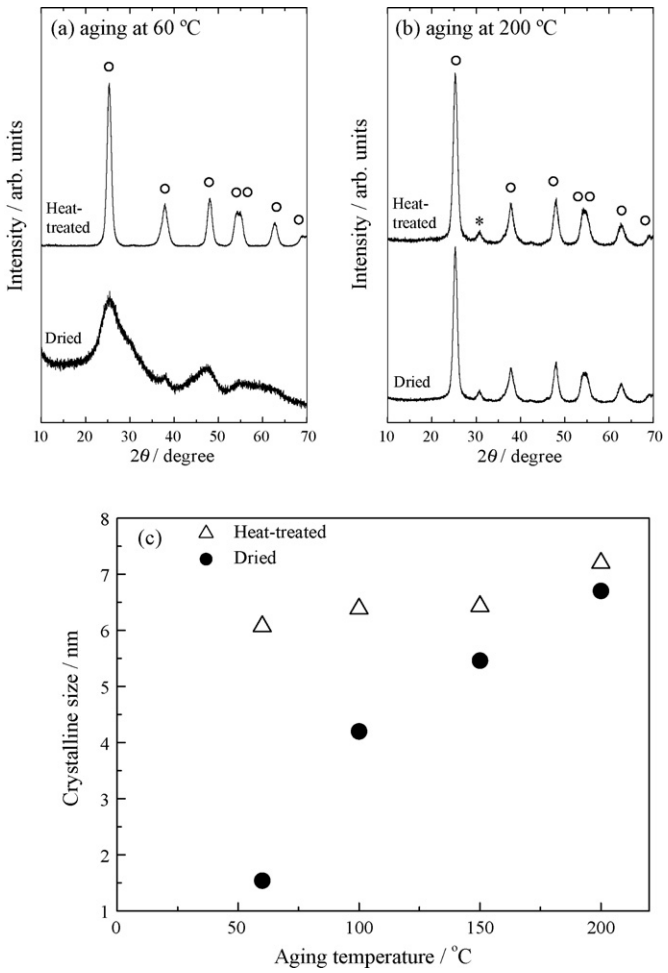

Fig. 2. XRD patterns of dried and heat-treated gels ($f = 0.750$) derived via aging at 60 °C (a) and those via aging at 200 °C (b). All the diffraction peaks (open circles) correspond to the anatase phase, except for that denoted by an astarisk (*), which is ascribed to the brookite phase. (c) The crystallite size of dried (closed circles) and heat-treated gels (open triangles) as a function of aging temperature. The crystallite sizes were evaluated from anatase 1 0 1 diffraction peaks using the Scherrer's equation.

temperature of aging treatment (see closed circles). As expected from the present synthesis condition, when the temperature of aging treatment is 60 °C that is the same as the temperature for gelation, the dried gel exhibits the crystallite size as small as 1.6 nm, reflecting the poor crystallinity. Increasing the aging temperature to 200 °C causes a gradual increase in crystallite size to 6.7 nm, indicating the improved crystallinity. It is also seen from Fig. 2c that the crystallite sizes of dried gels increase by heat treatment to 400 °C (see open triangles). For the heat-treated gels, the crystallite sizes lie in a range of 6–7 nm and are almost independent of the aging temperature. The crystallite growth during heat treatment occurs more significantly for the dried gels derived via aging treatment at lower temperatures. In particular, a drastic crystallite growth from 1.5 to 6.2 nm is observed when the dried gel derived via aging at 60 °C is directly subjected to the heat treatment (without additional high-temperature aging treatment). This result may be related to the surface state of the primary particles (crystallites) comprising the gel skeletons. In the as-gelled wet state, many unre-

[1] The XRD pattern of the dried gel derived via aging at 60 °C reveals the asymmetric shape of the diffraction peak at $2\theta = 25°$. The asymmetric broadening is presumably due to the overlapping of anatase 1 0 1 peak and brookite 1 1 1, 1 2 0, and 1 2 1 peaks. Due to the absence of other distinct anatase peaks, we determined the crystallite size of anatase TiO_2 from the left half of the peak at around $2\theta = 25°$ on the assumption that most of the peaks intensity was originated from the anatase phase.

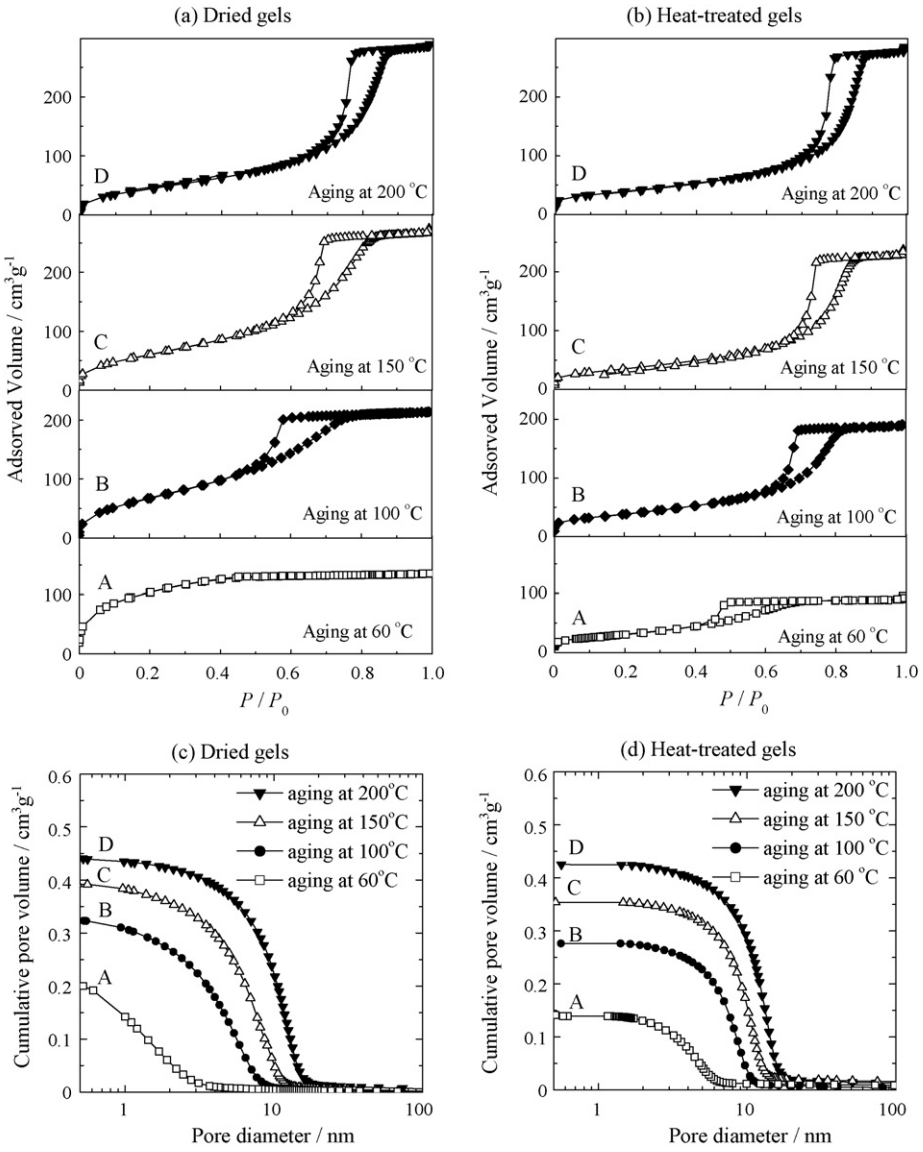

Fig. 3. Nitrogen adsorption–desorption isotherms of dried (a) and heat-treated gels (b) derived via aging treatment at 60 °C (□), 100 °C (♦), 150 °C (△), and 200 °C (▼); (c) and (d) represent the corresponding BJH pore size distributions of the dried and heat-treated gels, respectively.

acted groups would exist on the particle surface, resulting in the poor crystallinity. In the present case, most of the unreacted groups are considered to be hydroxyl groups, due to the nearly complete hydrolysis of titanium alkoxide. Since the condensation among hydroxyl groups proceeds even during the aging process after the gelation, the temperature of aging treatment inevitably affects the crystallite size and crystallinity. Aging treatments at lower temperatures result in more incomplete condensation of hydroxyl groups, and therefore, more rapid crystallite growth occurs by further condensation during subsequent heat treatment at 400 °C. In contrast, aging treatment at 200 °C allows the growth into well-crystallized particles with less hydroxyl groups, so that the crystallite growth is suppressed during the heat treatment at 400 °C. The minor growth of crystallite size by heat treatment (from 6.7 to 7.2 nm) as observed for the dried gel derived via aging treatment at 200 °C suggests that the crystallinity of gel skeletons is improved to a large extent under the milder temperature than that required for the heat treatment process.

Nitrogen physisorption measurements have been used to characterize the textural properties in gel skeletons of the dried and heat-treated gels prepared with $f = 0.750$ and aged at different temperatures, as obtained by adsorption–desorption isotherms (Fig. 3a and b), BJH pore size distributions (Fig. 3c and d), and BET surface area (Fig. 4a). The mean pore sizes, cumulative pore volumes, and BET surface areas obtained by nitrogen sorption analysis are summarized in Table 2, together with the crystallite sizes determined by XRD analysis. Table 2 also lists the linear shrinkage estimated by the size reduction relative to the ID of the polypropylene tube used for the gel synthesis. The dried gel derived via aging treatment at 60 °C exhibits the isotherm of type-I (Fig. 3a, A), signifying the existence of micropores. Upon direct heat treatment to 400 °C (without additional high-temperature aging treatment), the isotherm shape turns into that of type-IV with an H2 hysteresis loop (Fig. 3b, A), indicating the production of mesopores. The mesopore formation induced by direct heat treatment is also recognized in the corresponding pore size distribution curves. The dried gel derived via aging treatment at 60 °C exhibits a broad pore size distribution with a substantial percentage of micropores sized below 2 nm (Fig. 3c, A), while the heat-treated gel possesses a relatively sharp pore size distribution at around 4 nm (Fig. 3d, A). The collapse of micropores manifests itself in a large loss in BET surface area from 380 to 139 $m^2 g^{-1}$ (Fig. 4a and Table 2). A similar pore evolution

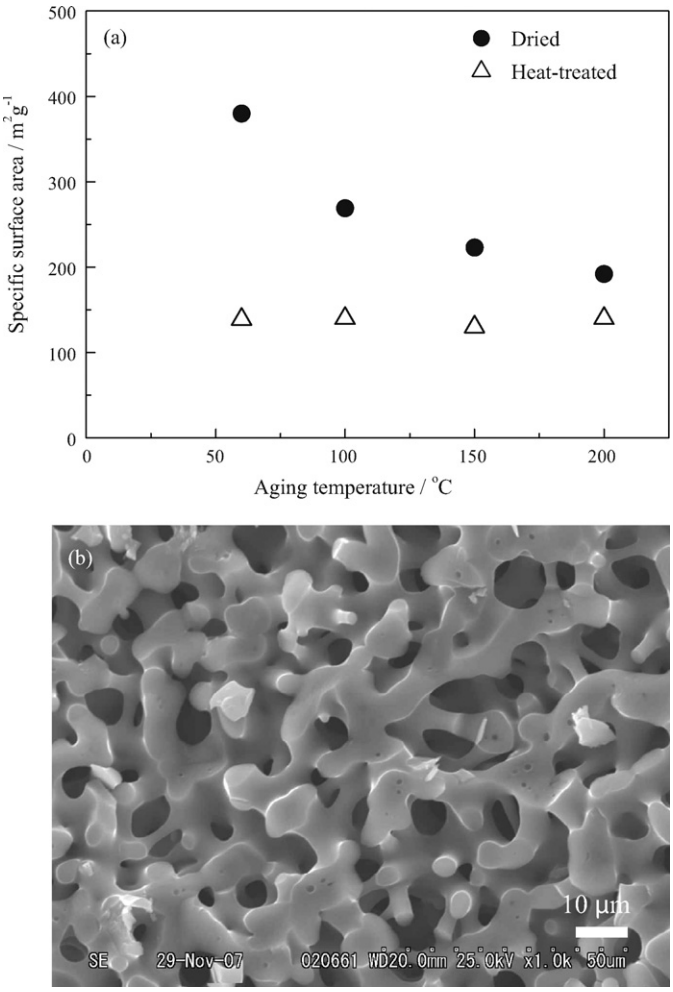

Fig. 4. (a) BET specific surface area of the dried (closed circles) and heat-treated gels (open triangles) as a function of aging temperature. (b) SEM image of the heat-treated gel prepared with $f = 0.750$ and aged at 200 °C. The scale bar corresponds to 10 μm.

was observed for the Ti(O^nPr)$_4$–FA system as reported previously [29,35], and ascribed to the significant crystallite growth during heat treatment, as observed for the dried gel derived via aging at 60 °C (see Fig. 2c). In other words, the particle growth enlarges the inter-particle voids to form the accessible mesopores. However, this approach allows only a restricted control over the mesoporours structures because the direct heat treatment process usually causes particles to form hard aggregates and yields extensive crystallite growth due to the increased degree of particle packing. This is reflected in the reduction of cumulative pore volume from 0.20 to 0.14 cm^3 g^{-1} during the direct heat treatment at 400 °C (Table 2 and Fig. 3c, A vs. Fig. 3d, A). We also confirmed that heat treatment to temperatures over 400 °C is not feasible without spoiling the mesoporosity.

In contrast, adopting aging treatment at higher temperatures than 60 °C as the post-gelation process enables more extensive control over the mesoporous structures, as revealed by nitrogen sorption analysis. The dried gels derived via aging treatment at 100, 150, and 200 °C exhibit a type-IV isotherm with an H2 hysteresis loop (Fig. 3a, B–D) and possess pore size distributions in the mesopore regime (Fig. 3c, B–D). These results imply that restructuring of microporous into mesoporous structures takes place during the high-temperature aging process. Interestingly, for these dried gels, both the pore size and pore volume gradually increase with increasing the aging temperature; the mean pore size and cumulative pore volume increase from less than 2 to 12.4 nm and from 0.20 to 0.44 cm^3 g^{-1}, respectively, when the temperature of aging treatment increases from 60 to 200 °C (see Table 2). Apart from the mesopore evolution, the increase in the aging temperature from 60 to 200 °C leads to the reduction of BET surface area from 380 to 192 m^2 g^{-1} for the dried gels (closed circles in Fig. 4a and Table 2). This is attributed to the stepwise crystallite growth during the aging treatment at elevated temperatures (see Fig. 2c) and concomitant collapse of the microporosity that yields high surface area. Obviously, the high-temperature aging treatment allows the enlargement of mesopore size up to over 10 nm, while gaining the mesopore volume. This is never achieved by the direct heat treatment process which leads to hard aggregation of particles. Since the aging treatment in the mother liquor at elevated temperatures can be regarded as a hydrothermal processing, the hard aggregation of primary particles in the gel skeletons is expected to be suppressed [36]. It is highly probable that loosely-packed particle assembly via coarsening during the high-temperature aging treatment is responsible for the pore size enlargement. In addition, more progressive condensation during the aging treatment at higher temperatures would support mechanically the mesoporous textures against the shrinkage of gel skeletons during evaporation drying, leading to the higher pore volume. Further investigations are needed to clarify the coarsening mechanism during the high-temperature aging treatment.

Nitrogen sorption analysis also shows that the mesotextures tailored by high-temperature aging treatment are retained after heat treatment to 400 °C (Fig. 3b, B–D). The heat-treated gels derived via aging at 100, 150, and 200 °C exhibit the increase in pore sizes and the reductions in cumulative pore volumes and BET surface areas relative to the original dried gels (Table 2 and Fig. 4a), although to a lesser extent than the heat-treated gel derived via aging treat-

Table 2
Textural properties of dried and heat-treated TiO_2 gels derived via aging at 60, 100, 150, and 200 °C. Linear shrinkage for the dried and heat-treated gels is also shown.

Aging temperature (°C)	Sample condition	Crystallite size[a] (nm)	Mean pore size[b] (nm)	Cumulative pore volume (<100 nm)[b] (cm^3 g^{-1})	BET specific surface area[b] (m^2 g^{-1})	Linear shrinkage[c] (%)
60	Dried	1.5	1.5	0.20	380	36
	Heat-treated	6.1	4.6	0.14	139	49
100	Dried	4.2	5.6	0.32	269	38
	Heat-treated	6.3	8.8	0.28	140	43
150	Dried	5.5	7.9	0.39	223	36
	Heat-treated	6.4	10.4	0.35	130	41
200	Dried	6.7	12.4	0.44	192	37
	Heat-treated	7.2	13.8	0.42	140	39

[a] Calculated from anatase 1 0 1 diffraction peaks in XRD patterns using the Scherrer's equation.
[b] Determined by the nitrogen sorption analysis.
[c] Estimated from the diameter of TiO_2 rods relative to the 6 mm ID of polypropylene tube used for the gel synthesis.

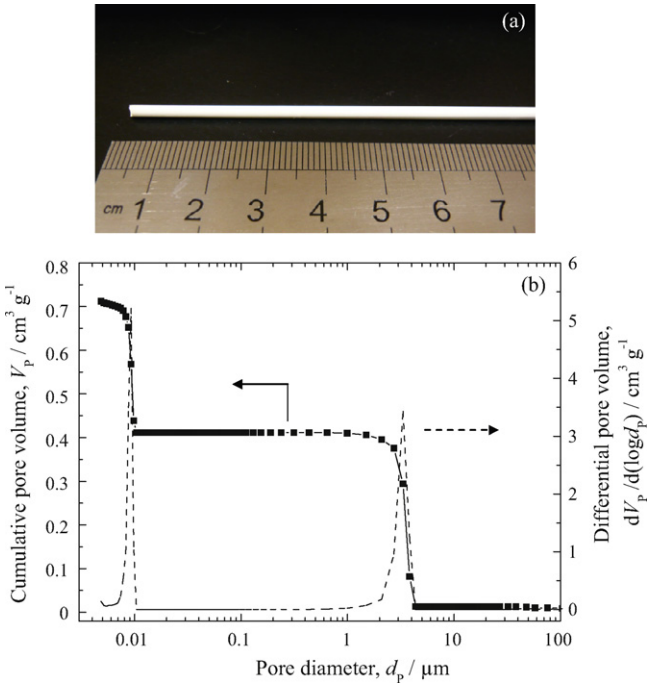

Fig. 5. (a) Photograph of monolithic TiO_2 rod (f = 0.750) derived via aging treatment at 200 °C and subsequent heat treatment at 400 °C. The monolithic rod was prepared in a polypropylene tube of 4 mm ID. (b) Pore size distribution of the monolithic TiO_2 gel (f = 0.750) derived via aging treatment at 200 °C and subsequent heat treatment at 400 °C, which was measured by using the mercury intrusion method.

ment at 60 °C does. In particular, only a slight increase in the pore size (from 12.4 to 13.8 nm) and little reductions in the pore volume (from 0.44 to 0.42 cm^3 g^{-1}) and BET surface area (from 192 to 140 m^2 g^{-1}) are observed when the dried gel derived via aging at 200 °C is subjected to the heat treatment. The excellent thermal stability is consistent with the minimal crystallite growth during the heat treatment, which is due to the fully improved crystallinity of the dried gel derived via aging treatment at 200 °C (see Fig. 2c). A remarkable feature observed for the heat-treated gels derived via aging at 100, 150, and 200 °C is that their mesopore size distributions (Fig. 3d, B–D) become narrower compared to those for the original dried gels (Fig. 3c, B–D), indicating the enhanced uniformity of mesopore sizes. The BET surface areas for the heat-treated gels lie in a range of 130–140 cm^2 g^{-1}, regardless of the aging temperature (see open triangles in Fig. 4a). All the above observations indicate that the heat treatment process causes the microporosity to almost completely collapse, without significantly affecting the mesoporous structures tailored by high-temperature aging treatment. As a result, the combination of high-temperature aging treatment and heat treatment allows us to create well-crystallized anatase TiO_2 skeletons with uniform pore size distributions with mesopore sizes up to about 14 nm. Here, it should be emphasized that the control over the mesoporous structures using high-temperature aging treatment is possible without spoiling the preformed micrometer-range morphology. A representative SEM image is shown in Fig. 4b. It is evident that the macroporous morphology is maintained even after the aging treatment at 200 °C and subsequent heat treatment at 400 °C.

3.3. Chromatographic separation of phosphorus-containing compounds

The TiO_2 monoliths with bimodal pore size distributions with controllable sizes in the meso- and macropore regimes are expected to find applications as chromatographic separation media if deformation of monolithic shape and/or crack formation in the gel skeletons can be minimized during evaporation drying and heat treatment. During evaporation drying, the micro- and mesopores existing in the gel skeletons develop high capillary pressures, resulting in the shrinkage of the gel. If the exterior surface of monolithic gel shrank much faster than the interior, the drying stress arising from the differential strain would cause cracking and deformation

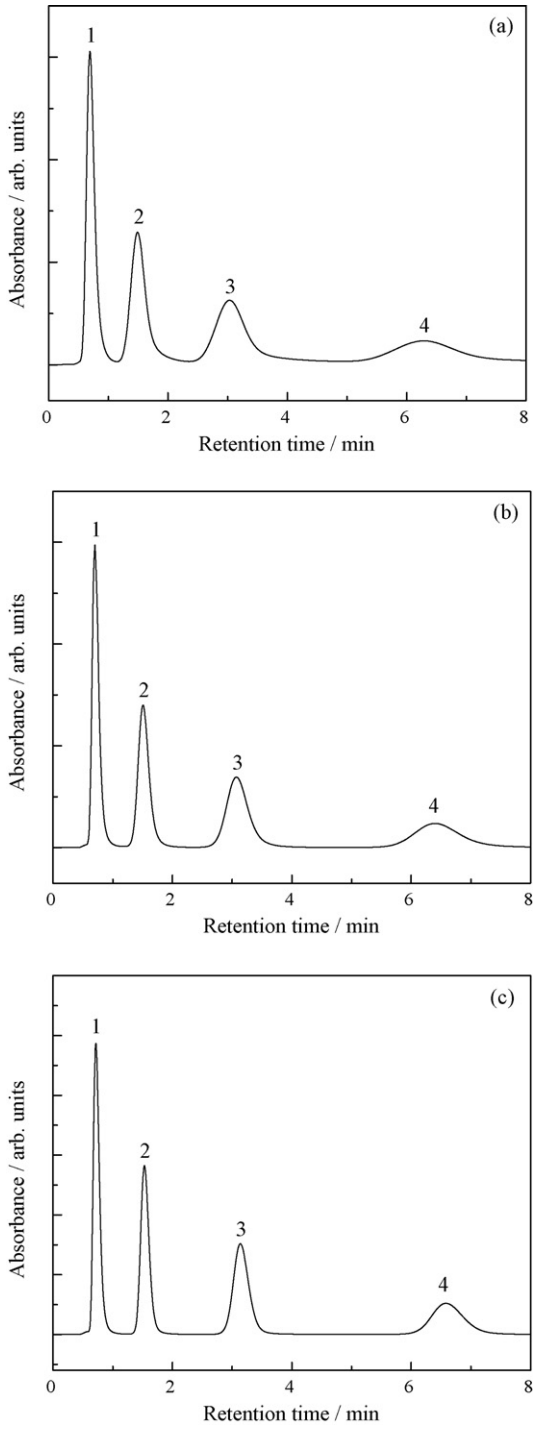

Fig. 6. Chromatograms of adenosine, AMP, ADP, and ATP using monolithic TiO_2 rod columns (2.4 mm ID and 50 mm length) prepared with f = 0.775 (a), 0.750 (b), and 0.725 (c). These monolithic rods were derived via the aging treatment at 200 °C and subsequent heat treatment at 400 °C. The sample mixture contains (1) adenosine, (2) AMP, (3) ADP, and (4) ATP. Mobile phase: 50 mM Na–Pi buffer (pH 6.5), 60% acetonitrile (v/v). Linear velocity: 1.2 mm s^{-1}. Detection: UV at 260 nm. Sample volume: 1 μl.

Table 3
Chromatographic characterization of TiO_2 rod columns prepared with f = 0.775, 0.750, and 0.725.

f = NFA/Ti(O^nPr)$_4$ (molar ratio)	Aging temp. (°C)	Macropore size[a] (μm)	Mesopore size[b] (nm)	Back pressure (MPa)	Theoretical plate (1/m)
0.775	200	5.2	13.8	0.8	2,820
0.750	200	3.3	12.5	0.8	6,100
0.725	200	1.6	12.0	1.6	13,120

[a] Determined by the mercury porosimetry.
[b] Determined by the nitrogen sorption analysis.

[37,38]. In the present system, however, the interconnected macropores increase the permeability of the gel to the flow of pore liquid, leading to less drying stress. In addition, the additional aging treatment at higher temperatures produces the larger and more uniform mesopores in the gel skeletons (see Fig. 3) so that the permeability of the gel can be further enhanced [37,38]. The most important thing is that the high-temperature aging treatment is effective in improving the mechanical strength of gel skeletons through the condensation among hydroxyl groups located on the particle surfaces, which makes the gel skeletons better able to withstand the capillary pressures developed during drying process. As a result, more uniform shrinkage and less cracking and deformation are expected especially for the dried gels derived via aging treatment at 200 °C. Moreover, just a little shrinkage is observed when the dried gel derived via aging at 200 °C is subjected to heat treatment at 400 °C (see Table 2). This observation is consistent with the experimental result that the mesotexture tailored by aging treatment at 200 °C exhibits the remarkable thermal robustness (see Fig. 3). For these reasons, we here have selected the heat-treated gels derived via aging at 200 °C as the chromatographic separation media for phosphorus-containing compounds.

Fig. 5a depicts the photograph of heat-treated TiO_2 rod prepared in a polypropylene tube of 4 mm ID. Although the gel shrinkage during the synthesis process leads to the size reduction of about 40% relative to the initial diameter of tube, no apparent cracking and warping are detected in the resultant TiO_2 rod. In this study, we have prepared the TiO_2 rods with different macropore sizes (1.6, 3.3, and 5.2 μm) but with nearly comparable mesopore sizes (12–14 nm), and examined the dependence of the macroporous structures on chromatographic separation. As described above, the macropore size is controlled by varying the amount of NFA in the starting composition, while the mesopores with sizes over 10 nm form during the aging treatment at 200 °C after the gelation. Fig. 5b displays the pore size distribution over the meso- to macroporous regimes measured for the monolithic TiO_2 rod (f = 0.750) using the mercury porosimetry. One can see that the monolithic TiO_2 rod possesses a bimodal porous structure with relatively sharp pore size distributions in the meso- and macroporous regimes. The chromatograms of TiO_2 rod columns prepared with f = 0.775, 0.750, and 0.725 and then clad with FEP poly(tetrafluoroethylene) are shown in Fig. 6a, b, and c, respectively. A mixture of adenosine, AMP, ADP, and ATP was used as a sample. In contrast to the SiO_2 rod column that has no ability to separate these phosphates [25], all the TiO_2 rod columns exhibit the separation efficiency due to their ability to bind phosphate group. It is found that the retention time increases with an increase in the number of the phosphate groups. The theoretical plates and back pressures are listed in Table 3, together with the macro- and mesopore sizes of the TiO_2 columns. Since the separation efficiency depended on the kind of solutes, the theoretical plate was evaluated by using the peak of ATP. The theoretical plate becomes larger as the macropore size decreases. The smaller macropore sizes, under comparable macropore volumes, correspond to the thinner gel skeletons, resulting in higher separation efficiency. This is similar to the effect observed for the conventional particle-packed columns in which smaller particles lead to better separation efficiency; however, a higher back pressure is needed for faster analysis. Here, it should be noted that the height equivalent to a theoretical plate (HETP) for the present TiO_2 rod column (f = 0.725) is larger than that for the TiO_2 capillary column of 75 μm ID as reported by Randon et al. [33] (76 μm vs. 15–30 μm), indicating the lower separation efficiency for the present rod column. This may be partly due to the existence of some preferential flow paths inside the rod columns resulting either from our cladding procedure or from inhomogeniety in the macroporous network of our monoliths. These two factors, i.e., the cladding procedure and the inhomogeniety in macroporous network, also would influence the variation of back pressure with the macropore size; the decrease in macropore size from 5.2 to 1.6 μm brings about an increase in the back pressure by a factor of 2, which is lower than that expected from the size reduction. Recent computational study has revealed that a slight variance of the skeleton thickness and macropore size of monolithic columns severely hampers the possibility to obtain well-performing columns [39]. Although the synthesis process and cladding procedure have to be further improved in the future, the present research unambiguously demonstrates that the TiO_2 rod columns are applicable as the separation media for the phosphate compounds. To the best of our knowledge, this is the first demonstration of chromatographic separation of phosphate compounds using pure TiO_2 monolithic columns. The developed method could be applied to measure APTase activity of proteins by analyzing the amount of ADP produce by the ATPase reaction [16]. The TiO_2 rod columns are expected to have potential applications for fast separations of phosphorylated biomolecules, including sugar phosphates [17], herbicides [18], and proteins [19]. Furthermore, the design of porous structures may provide a route for high-throughput screening to pre-concentrate the phosphate compounds.

4. Conclusions

Anatase TiO_2 monolithic gels with well-defined bicontinuous macropores and microstructured skeletons have been prepared via the alkoxy-derived sol–gel process in the presence of NFA and PEO under strongly acidic conditions, and the micro- and mesotextures and crystallinity of the gel skeletons have been tailored by utilizing high-temperature aging treatment as a post-gelation process. Adjusting the amounts of NFA and PEO in the starting solution allows concurrence of polymerization-induced phase separation and gelation, and produces large-dimension TiO_2 monoliths with controllable macroporous morphology. Aging treatment of the wet gels in the mother liquor at temperatures between 100 and 200 °C results not only in the formation of mesoporous structures but also in the improvement of crystallinity, without spoiling the preformed macroporous morphology. Depending on the aging temperature, the mesopore size can be enlarged up to about 13 nm, while gaining the mesopore volume. Subsequent heat treatment to 400 °C makes the pore size distributions narrower and further enhances the crystallinity of gel skeletons. The present synthetic process thus enables us to produce crack-free, well-crystallized anatase TiO_2 monoliths having bimodal meso-macroporous structures with adjustable pore sizes and uniform pore size distributions. Using pure TiO_2 rod columns with bimodal macro–mesoporous structures, chro-

matographic separation of phosphorus-containing compounds is successfully demonstrated, indicating the homogeneous structural integrity.

Acknowledgements

This study was financially supported by a Grant for Practical Application of University R&D Results under the Matching Fund Method from the New Energy and Industrial Technology Development Organization (NEDO), Japan. K.F. appreciates the research grants from the Inamori Foundation and Kurata Memorial Hitachi Science and Technology Foundation.

References

[1] F. Svec, E.C. Peters, D. Sykora, C. Yu, J.M.J. Frecht, J. High Resolut. Chromatogr. 23 (2000) 3.
[2] N. Tanaka, H. Kobayashi, K. Nakanishi, H. Minakuchi, N. Ishizuka, Anal. Chem. 73 (2001) 420A.
[3] K. Nakanishi, J. Porous Mater. 4 (1997) 67.
[4] H. Minakuchi, K. Nakanishi, N. Soga, N. Ishizuka, N. Tanaka, Anal. Chem. 68 (1996) 3498.
[5] H. Minakuchi, K. Nakanishi, N. Soga, N. Ishizuka, N. Tanaka, J. Chromatogr. A 762 (1997) 135.
[6] J. Nawrocki, C. Dunlap, A. McCormick, P.W. Carr, J. Chromatogr. A 1028 (2004) 1.
[7] J. Nawrocki, C. Dunlap, L. Li, J. Zhao, C.V. McNeff, A. McCormick, P.W. Carr, J. Chromatogr. A 1028 (2004) 31.
[8] K. Tani, Y. Suzuki, J. Chromatogr. A 722 (1996) 129.
[9] H. Matsuda, H. Nakamura, T. Nakajima, Anal. Sci. 6 (1990) 911.
[10] Y. Ikeguchi, H. Nakamura, Anal. Sci. 16 (2000) 541.
[11] M.P. Lingney, E.F. Funkenbushe, P.W. Carr, J. Chromatogr. 499 (1990) 291.
[12] J. Randon, P. Blanc, R. Peterson, J. Membr. Sci. 98 (1995) 119.
[13] Y. Ikeguchi, H. Nakamura, Anal. Sci. 13 (1997) 479.
[14] I. Kuroda, Y. Shintani, M. Motokawa, S. Abe, M. Furuno, Anal. Sci. 20 (2004) 1313.
[15] A. Sano, H. Nakamura, Anal. Sci. 20 (2004) 565.
[16] Y. Kimura, S. Shibasaki, K. Morisato, N. Ishizuka, H. Minakuchi, K. Nakanishi, M. Matsuo, T. Amachi, M. Ueda, K. Ueda, Anal. Biochem. 326 (2004) 262.
[17] Y. Sekiguchi, N. Mitsuhashi, Y. Inoue, H. Yagisawa, T. Mimura, J. Chromatogr. A 1039 (2004) 71.
[18] T. Ishiwata, K. Takai, H. Okada, K. Ohashi, Jpn. J. Forensic Toxicol. 22 (2004) 7.
[19] K. Hata, H. Morisaka, K. Hara, J. Mima, N. Yumoto, Y. Tatsu, M. Furuno, N. Ishizuka, M. Ueda, Anal. Biochem. 350 (2006) 292.
[20] M.W. Pinkse, P.M. Uitto, M.J. Hihorst, B. Oomes, A.J. Heck, Anal. Chem. 76 (2004) 3935.
[21] M.R. Larsen, T.E. Thingholm, O.N. Jensen, P. Roepstorff, T.J. Jorgensen, Mol. Cell. Proteomics 4 (2005) 873.
[22] H.K. Kweon, K. Hakansson, Anal. Chem. 78 (2006) 1743.
[23] N. Sugiyama, T. Masuda, K. Shinoda, A. Nakamura, M. Tomita, Y. Ishihama, Mol. Cell. Proteomics 6 (2007) 1103.
[24] Z.-G. Shi, Y.-Q. Feng, L. Xu, M. Zhang, S.-L. Da, Talanta 63 (2004) 593.
[25] S. Miyazaki, M.Y. Miah, K. Morisato, Y. Shintani, T. Kuroha, K. Nakanishi, J. Sep. Sci. 28 (2005) 39.
[26] K. Fujita, J. Konishi, K. Nakanishi, K. Hirao, Appl. Phys. Lett. 85 (2004) 5595.
[27] D.C. Hoth, J.G. Rivera, L.A. Colón, J. Chromatogr. A 1079 (2005) 392.
[28] J. Konishi, K. Fujita, K. Nakanishi, K. Hirao, Chem. Mater. 18 (2006) 864.
[29] J. Konishi, K. Fujita, K. Nakanishi, K. Hirao, Chem. Mater. 18 (2006) 6069.
[30] J. Konishi, K. Fujita, S. Oiwa, K. Nakanishi, K. Hirao, Chem. Mater. 20 (2008) 2165.
[31] S. Backlund, J.-H. Smått, J.B. Rosenholm, M. Lindén, J. Disper. Sci. Technol. 28 (2007) 115.
[32] J. Randon, S. Huguet, A. Piram, G. Puy, C. Demesmay, J.-L. Rocca, J. Chromatogr. A 1109 (2006) 19.
[33] J. Randon, J.-F. Guerrin, J.-L. Rocca, J. Chromatogr. A 1214 (2008) 183.
[34] B. Siffert, J. Li, Colloids Surf. 40 (1989) 207.
[35] J. Konishi, K. Fujita, K. Nakanishi, S. Nishitsuji, M. Takenaka, K. Miura, K. Hirao, J. Sol–Gel Sci. Technol. 46 (2008) 63.
[36] C.-C. Wang, J.Y. Ying, Chem. Mater. 11 (1999) 3113.
[37] G.W. Scherer, J. Non-Cryst. Solids 100 (1988) 77.
[38] G.W. Scherer, J. Am. Ceram. Soc. 73 (1990) 3.
[39] J. Billen, P. Gzil, G.V. Baron, G. Desmet, J. Chromatogr. A 1077 (2005) 23.